

ANALYSIS OF GRADED BAND GAP SOLAR CELLS WITH SCAPS

Marc Burgelman and Jonas Marlein

University of Gent, Electronics and Information Systems (ELIS), Pietersnieuwstraat 41, B-9000 Gent, 'Belgium'
phone: 00 32 9 2643381; e-mail: Marc.Burgelman@elis.ugent.be

ABSTRACT: To simulate the complicated, graded structure of modern thin film CIGS solar cells, we followed a 'material driven' approach. Each layer is considered as a compound $A_{1-y}B_y$; the desired composition grading $y(x)$ over a layer is set; all materials properties are specified for the pure materials A and B; finally, the local materials properties are derived from the local composition. This strategy was implemented in our thin film solar cell simulation software SCAPS.

The new facility was used to study CIGS based thin film solar cells with a graded absorber layer. We showed that a grading strategy with a Ga-poor bulk and narrow Ga-rich layers at both ends of the absorber can indeed lead to a more favourable trade-off between J_{sc} and V_{oc} than can be obtained with uniform CIGS absorbers. However, this result depends on the specific assumptions on recombination.

Keywords: Thin Film Solar Cell; CIGS; Modelling; Software.

1 INTRODUCTION

In traditional thin film solar cells, the absorber materials are engineered to have an optimised band gap energy E_g : this is the well known trade-off between high current for low E_g and high voltage for high E_g . Modern thin film $\text{Cu}(\text{In,Ga})(\text{Se,S})_2$ or CIGS based solar cell structures however use more complicated band gap strategies, almost always involving a grading of the band gap $E_g(x)$ and most other materials properties in the cell thickness direction x . This is achieved by introducing a spatial variation of the Ga and/or S content within the CIGS layer. Such grading is present in the record $> 19\%$ efficient CIGS cells of NREL [1], and in CIGS cells and modules now prepared for industrialisation by AVANCIS [2], Würth Solar [3] and others. The underlying idea is that it should be possible to increase the short circuit current while maintaining the open circuit voltage by realising a well suited band gap profile $E_g(x)$. To assist the understanding and designing of these advanced CIGS solar cells, the inclusion of band gap grading in solar cell simulation programmes in use by the thin film solar cell research community becomes increasingly important. There are literature reports on simulations of CIGS solar cells with graded band gap, e.g. [4][5], but not with simulation tools that are open or easily accessible to the PV public.

In this paper we introduce the implementation of graded band gaps in SCAPS, a solar cell simulation programme developed by the University of Gent, and well spread in thin film solar cell labs, especially for the study of CIGS and CdTe based cells [6]. The general purpose of this work is to offer a user programme capable of calculating graded structures to the thin film PV research community. A more specific purpose is to apply then this tool to thin film CIGS solar cells.

2. APPROACH AND METHODS

It should be noted that by implementing a graded composition of the cell layers, not only the band gap $E_g(x)$, but almost all other materials properties become graded: electron affinity $\chi(x)$, optical absorption $\alpha(x, \lambda)$, effective density of states $N_C(x)$ and $N_V(x)$, doping

density $N_C(x)$ and $N_A(x)$, transport properties $\mu_n(x)$ and $\mu_p(x)$, recombination properties $N_t(x)$, $\sigma_n(x)$, $\sigma_p(x)$,...

A simulation tool including grading thus should take everywhere the position dependent value of the materials parameters. It is not trivial at all to implement this in a way that is convenient for the user and efficient for the internal operation of the programme. A more scientific consequence of grading is that it is modifying the semiconductor equations governing the problem. In a problem with uniform layers, the driving forces for electrical current are the electrostatic potential gradient $\nabla\Phi$ (drift current) and the concentration gradients ∇n and ∇p (diffusion current). When grading is present, extra driving terms should be added: the gradient of the electron affinity $\nabla\chi$, the gradient of the band gap ∇E_g , and the gradients of the effective density of states in the conduction and valence bands: $\nabla(\log N_C)$ and $\nabla(\log N_V)$. Also, the electron and hole continuity equations are modified by the presence of a mobility gradient $\nabla\mu_n$ or $\nabla\mu_p$, and the Poisson equation is modified by a gradient $\nabla\epsilon$ in dielectric constant. These modified equations have been described in the literature [4][5][7][8] and are now implemented and solved in SCAPS.

3. IMPLEMENTATION IN SCAPS

SCAPS [6] uses an exponentially fitted discretisation scheme to set up the equations for the electron and hole current J_n and J_p , and for the continuity equation for electrons and holes, involving the Bernoulli function $B(x)$ [9]. When gradients in electron affinity χ or band gap E_g are present, this formalism is extended by adding the 'band potentials' ϑ_n and ϑ_p to the electrostatic potential Φ [8]. One obtains an expression for the currents at a point $i + \frac{1}{2}$ halfway between two mesh points x_i and x_{i+1} :

$$J_{n,i+1/2} = \frac{D_{n,i+1/2}}{x_{i+1} - x_i} \cdot \left[B(\Phi_i^n - \Phi_{i+1}^n) n_i - B(\Phi_{i+1}^n - \Phi_i^n) n_{i+1} \right] \quad (1)$$

$$J_{p,i+1/2} = \frac{D_{p,i+1/2}}{x_{i+1} - x_i} \left[B(\Phi_i^p - \Phi_{i+1}^p) p_i - B(\Phi_{i+1}^p - \Phi_i^p) p_{i+1} \right] \quad (2)$$

Here $D_{n,i+1/2}$ and $D_{p,i+1/2}$ are the electron and hole diffusion constants evaluated halfway the interval ($i, i+1$), n and p the carrier concentrations, and Φ^n and Φ^p the effective electrostatic potentials evaluated at the mesh points i and $i+1$. These effective potentials are given by:

$$\Phi^n = \Phi + \mathfrak{G}_n \text{ with } \mathfrak{G}_n = \chi + \ln(N_C/N_{C0}) \quad (3)$$

$$\Phi^p = \Phi + \mathfrak{G}_p \text{ with } \mathfrak{G}_p = \chi + E_g - \ln(N_V/N_{V0}) \quad (4)$$

Here N_{C0} and N_{V0} are arbitrarily chosen reference values for the density of states N_C in the conduction band and N_V in the valence band. All potentials and energies occurring in Eq. (1) to (4) are normalised to kT/q or kT . There is no particular difficulty in adapting the discretised Poisson equation to a graded, thus x -dependent, dielectric constant $\varepsilon(x)$, and the discretised electron and hole continuity equations to graded diffusion constants $D_n(x)$ and $D_p(x)$.

To give a suitable and materials oriented description of the grading of the various materials parameters, we have chosen to derive all parameters consistently from the composition grading of a layer. Each layer is assumed to have composition $A_{1-y}B_y$. The user defines the properties of the pure compounds A (e.g. A = CuInSe₂) and B (e.g. B = CuInS₂), and the composition grading $y(x)$ over the thickness of the layer: thus defining the composition values y at the left and right side of the layer, and by specifying some grading law in between. All materials properties P are then derived from the local composition parameter $y(x)$, that is, $P[y(x)]$ is evaluated.

Several grading laws are implemented in SCAPS and offered by the user interface: linear, logarithmic, parabolic, power law, exponential, effective medium and a Beta function. These grading laws can be used to set the composition grading $y(x)$ over a layer, as well as to set the composition dependence $P(y)$ of a property. The following properties can be graded in SCAPS: E_g , χ , ε , N_C , N_V , μ_n , μ_p , v_{thn} , v_{thp} , N_D , N_A , N_t and $\alpha(\lambda)$.

The simplest grading law is linear; a linear dependence of a property P on composition y is sometimes called Vegard's law. An example of a parabolic dependence is the variation of the band gap with composition $E_g(y)$:

$$E_g(y) = (1-y)E_{gA} + yE_{gB} - b \cdot y(1-y) \quad (5)$$

where E_{gA} and E_{gB} are the band gaps of the pure materials A and B, and b is the bowing factor. The parameters E_{gA} , E_{gB} and b can be found in the literature for many material systems, e.g. [11] for the CuInSe₂-CuGaSe₂ system. The logarithmic, power and Beta function [12] laws are a kind of general purpose interpolation laws. The effective medium interpolation by Bruggeman is specially suited for the dielectric constant $\varepsilon(y)$, see e.g. [13]. An exponential law for composition grading $y(x)$ is well suited to describe a background composition in the bulk of a layer, with in- or out-diffusion at the layer boundaries. It has four parameters,

the composition y_{left} at $x = 0$ and y_{right} at $x = d$, the background or bulk composition y_0 and the characteristic length L . It takes the form:

$$y(x) - y_0 = \frac{(y_{\text{left}} - y_0) \sinh((d-x)/L) + (y_{\text{right}} - y_0) \sinh(x/L)}{\sinh(d/L)} \quad (6)$$

To interpolate the optical absorption constant $\alpha(\lambda, y)$ for some composition between the pure material A with composition $y = 0$ and absorption $\alpha_A(\lambda)$, and the pure material B with composition $y = 1$ and absorption $\alpha_B(\lambda)$, we developed the following algorithm. First, determine the cut-off wavelengths λ_{gA} and λ_{gB} of the pure materials, and a characteristic wavelength λ_{0A} and λ_{0B} in the near UV wavelength range. Usually, the $\alpha(\lambda)$ curves have a maximum (peak) in the near UV, if not one can take an arbitrary value for λ_{0A} and λ_{0B} . Then determine the cut-off wavelength λ_g of the compound with composition y with Eq. (5) and $\lambda_g \cong 1240 \text{ nm} \cdot \text{eV}/E_g$, and the UV peak wavelength λ_0 from e.g. linear interpolation between λ_{0A} and λ_{0B} . A first estimation for $\alpha(\lambda)$ is then obtained by evaluation α_A at a wavelength λ_A given by

$$\lambda_A = \frac{\lambda_{gA}(\lambda - \lambda_0) + \lambda_{0A}(\lambda_g - \lambda)}{\lambda_g - \lambda_0} \quad (7)$$

A second estimation is found by evaluation α_B at a wavelength λ_B found in a way similar to Eq. (7). Then take a weighted logarithmic average between the two estimations:

$$\log \alpha = (1-y) \cdot \log \alpha_A(\lambda_A) + y \cdot \log \alpha_B(\lambda_B) \quad (8)$$

We checked that this procedure gives acceptable results for the well known material system GaAs – AlAs. An example of such an alpha-interpolation result is shown in Fig. 1, where material A is pure CuInSe₂ with $\alpha(\lambda)$ data from Alonso [14], and material B is CuIn_{0.6}Ga_{0.4}Se₂, with $\alpha(\lambda)$ data from Malmström [15].

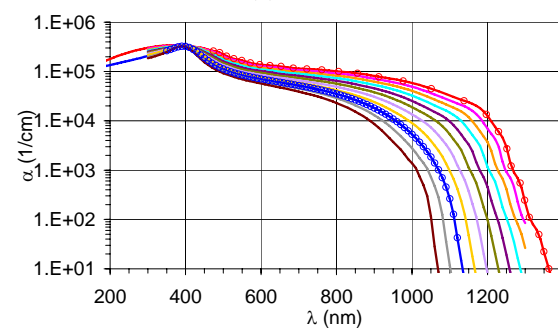


Fig. 1 SCAPS inter- and extrapolation of the optical absorption coefficient. Red dots: material A = CuInSe₂ [14]; blue dots: material B = CuIn_{0.6}Ga_{0.4}Se₂ [15]. The composition y of CuIn_{1-y}Ga_ySe₂ is varied: $y = 0, 0.05, 0.1, \dots, 0.50$ (solid lines).

Fig. 2 shows an example of a SCAPS solution of a simple grading problem. There is only one layer, and the only graded property is the dielectric constant ε . One can see in the energy band diagram (bottom of Fig. 2) that the drop in electrostatic potential, which can be seen as the

$E_C(x)$ profile, is entirely over the region with the low ϵ value, not over the region with high ϵ .

Another one layer example is Fig. 3 where three properties relevant to the valence band are graded. The composition is linearly graded, and E_g , χ and N_V depend on the composition: parabolically for E_g , linearly for χ and logarithmically for N_V (numerical values in the caption of Fig. 3). In this equilibrium band diagram, the Fermi level is flat. The valence band edge $E_V(x)$ is underneath E_F by an energy distance $kT \ln(N_V/N_A)$, and is in this case thus only determined by the grading valence band density of states $N_V(x)$. The grading of the conduction band follows then from $E_C(x) = E_V(x) + E_g(x)$. The grading of these properties E_g , χ and N_V causes an internal electric field, as follows from the drop in electrostatic potential, which is a replica of the vacuum reference level $E_C(x) + \chi(x)$. The diagram of Fig. 3 is calculated by SCAPS, and it confirms our common understanding on grading outlined above.

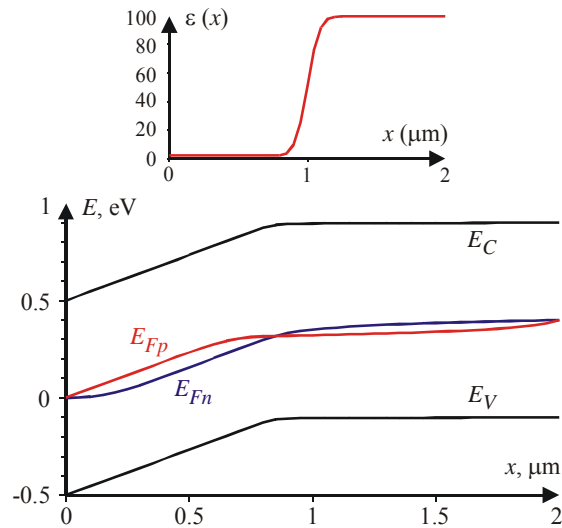


Fig. 2 Layer with graded $\epsilon(y)$. Top: the dielectric constant is graded from $\epsilon = 2$ left to $\epsilon = 100$ right, with a Beta-function grading law. Bottom: the energy bands in dark at $V = 0.4$ V.

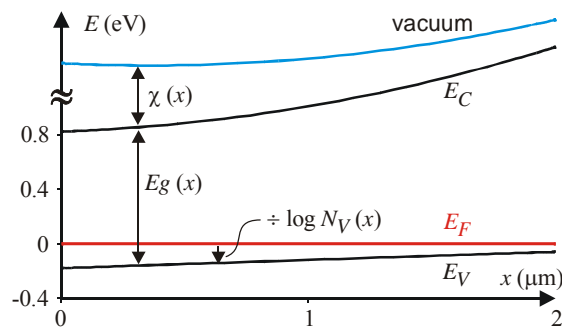


Fig. 3 Energy band diagram of a layer with linearly graded valence band properties, at equilibrium ($V = 0$; dark). $E_g(x)$ is parabolically graded from 1 eV left to 1.5 eV right, with $b = 0.5$ eV; $\chi(x)$ linearly from 4.5 eV left to 4.2 eV right and $N_V(x)$ logarithmically from 10^{19} cm^{-3} left to 10^{17} cm^{-3} right.

All algorithms discussed above have been implemented in SCAPS version 2.8, and the user interface has been extended to handle and visualise graded

problems and parameters. Also, all parameters concerning grading can be scanned in the batch mode. This extended SCAPS version is available to the scientific PV community.

4. RESULTS ON GRADED CIGS SOLAR CELLS

We start from the parameter set proposed in [16] to simulate a $\text{ZnO:Al}/i\text{-ZnO}/\text{CdS}/\text{SDL}/\text{Cu}(\text{In,Ga})\text{Se}_2/\text{Mo}$ structure, where SDL is a thin surface defect layer.

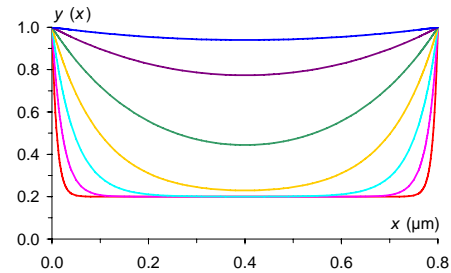


Fig. 4 Composition grading $y(x)$ of the CIGS layer used in the simulations of Fig. 5 and Fig. 6. The profile is 'exponential' with $y_{\text{left}} = y_{\text{right}} = 1$, $y_0 = 0.2$. The characteristic length L is logarithmically varying in 7 steps from $0.01 \mu\text{m}$ (red) to $1.00 \mu\text{m}$ (blue).

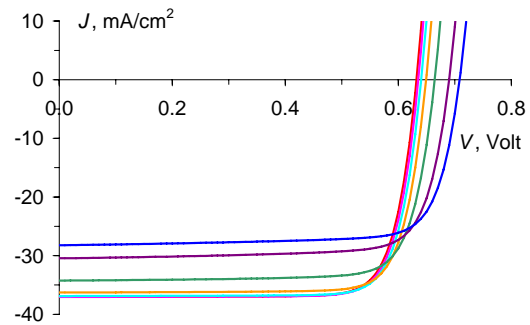


Fig. 5 SCAPS I - V simulation of cells with a graded CIGS layer. The composition profiles $y(x)$ of the different CIGS layer is as in Fig. 4, with the same colour code.

Here we consider all layers to be uniform, except the $0.8 \mu\text{m}$ thick CIGS layer which has a composition grading between the chalcopyrite compounds CuInSe_2 as 'pure A, $y = 0$ ' and $\text{CuIn}_{0.6}\text{Ga}_{0.4}\text{Se}_2$ as 'pure B, $y = 1$ '. The grading is of SCAPS type 'exponential' with the pure B material $y = 1$ left and right, and a bulk composition $y_0 = 0.2$, thus corresponding to $\text{CuIn}_{0.92}\text{Ga}_{0.08}\text{Se}_2$, and a varying characteristic length L to describe the composition diffusion at both ends of the absorber (Fig. 4). The only graded property is the band gap $E_g(y)$ with a composition dependence as in Eq. (5) with parameter values from [11]. In contrast to [16], a high surface recombination velocity $S_n = 10^6$ cm/s is set at the back contact (the Mo contact), and an interface recombination $S_i = 10^4$ cm/s at the CIGS/SDL interface.

Fig. 5 and Fig. 6 give the SCAPS simulations of the I - V curves and of the quantum efficiency QE , respectively. Fig. 5 illustrates the traditional trade-off between high J_{sc} and low V_{oc} at a low band gap composition $y = 0.2$ (red curves in Fig. 4, 5 and 6), and lower J_{sc} and higher V_{oc} at the higher band gap composition $y \rightarrow 1$ (blue curves).

The conclusion is that the Ga-content should be low over most of the CIGS bulk, but high in a narrow region at the back contact and at the interface; a characteristic width < 50 nm seems to be sufficient to combine high J_{sc} with high V_{oc} .

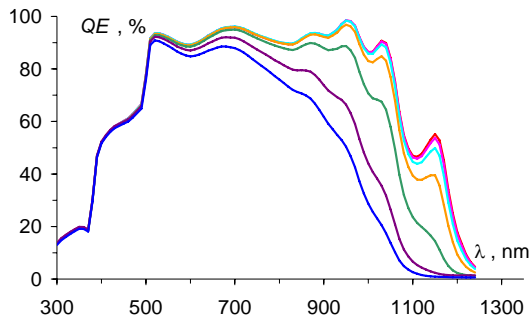


Fig. 6 SCAPS QE simulation of cells with a graded CIGS layer. The composition profiles $y(x)$ of the different curves is as in Fig. 4, with the same colour code.

We now consider the grading at both ends of the absorber separately. In the case of ‘back grading’, the composition is uniform and Ga-poor ($y = 0.2$) over all of the absorber, except for a narrow layer with characteristic width $L = 20$ nm at the back contact. The composition y_{back} at the back contact is varied. This composition profile is shown in Fig. 7 (discard the front grading shown at the right side of the figure). The corresponding I - V curves are shown in Fig. 8. It is obvious that a Ga rich layer at the back contact increases V_{oc} with nearly 100 mV. Such improvement is only obtained if surface recombination at the back contact is significant. When we set $S_n = 10^2$ cm/s instead of 10^6 cm/s, no effect of Ga enhancement at the back contact can be seen.

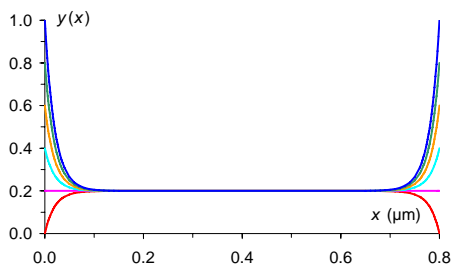


Fig. 7 Composition grading $y(x)$ of the CIGS layer used in the simulations of Fig. 8 and Fig. 9. The profile is ‘exponential’ with $y_0 = 0.2$, $L = 0.02$ μm and y_{left} (back) or y_{right} (front) linearly varying in 6 steps from 0 (red) to 1 (blue).

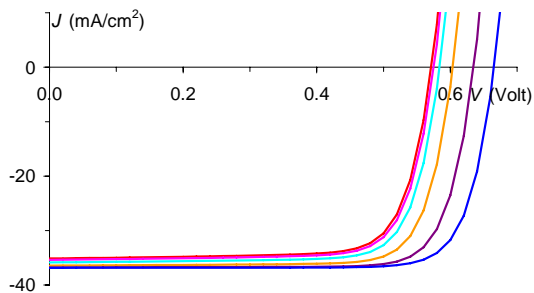


Fig. 8 SCAPS I - V simulation of cells with a ‘back-graded’ CIGS layer. The composition profiles $y(x)$ of the different curves is as in Fig. 7, with the same colour code.

In the case of ‘front grading’, the composition is uniform and Ga-poor ($y = 0.2$) over all of the absorber, except for a narrow layer with characteristic width $L = 20$ nm at the interface with the SDL. There, the composition y_{front} is varied. This composition profile is shown in Fig. 7 (discard the back grading shown at the left side of the figure). The corresponding I - V curves are shown in Fig. 9. When no interface states are present ($S_i = 0$) at the CIGS/SDL interface, no effect of front grading is seen at all (open circles in Fig. 9). However, when $S_i = 10^4$ cm/s,

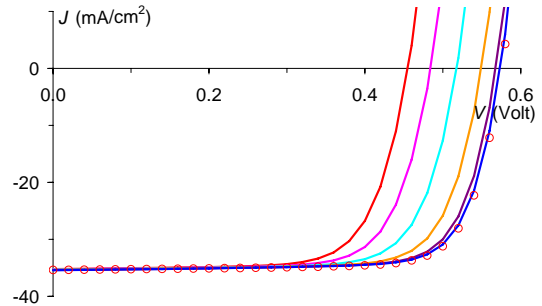


Fig. 9 SCAPS I - V simulation of cells with a ‘front-graded’ CIGS layer. The composition profiles $y(x)$ of the different curves is as in Fig. 7, with the same colour code. The open circles are for $S_i = 0$, all compositions y_{front} . The solid lines are for $S_i = 10^4$ cm/s.

a Ga rich layer at the front interface increases V_{oc} with nearly 120 mV. At $y_{front} = 1$ (thus when the composition is $\text{CuIn}_{0.6}\text{Ga}_{0.4}\text{Se}_2$), the effect of interface states is completely passivated.

A conclusion from this preliminary study is that the Ga-content should be as low as possible in the bulk of the CIGS, and that there should be an as narrow as possible Ga richer layer at both ends of the absorber. However, such a Ga-rich layer is only necessary if recombination at its position (back or front) is a substantial portion of the total recombination. Also, there is little doubt that this conclusion is also dependent on the assumptions on recombination in the CIGS bulk.

5. CONCLUSIONS

The complicated, graded structure of modern thin film CIGS solar cells necessitates an enhancement of user simulation programmes to include grading effects. We followed a ‘material driven’ methodology: the user can set a desired composition grading $y(x)$ over a layer, and then all materials properties are derived from the local composition. We extended our thin film solar cell simulation software SCAPS. This involved a new data structure, implementation of differential equations adapted for grading, and extensions to the graphical user interface which offers and visualises now a variety of grading laws for the composition profile $y(x)$ and the dependence $P(y)$ of many material properties on composition.

This new facility was used to study the effect of a CIGS absorber grading in CIGS based thin film solar cells. We showed that a grading strategy with a Ga-poor bulk and narrow Ga-rich layers at both ends of the absorber can indeed lead to a more favourable trade-off between J_{sc} and V_{oc} than can be obtained with uniform CIGS absorbers. However, this result depends on the

specific assumptions on recombination in the CIGS bulk and at both of its interfaces.

electrical modelling of Cu(In,Ga)Se₂ solar cells”, *Optical and Quantum Electronics*, **38** (12-14), 1115–1123, 2006.

ACKNOWLEDGEMENT

This work is part of the European Integrated Project ‘Athlet’.

REFERENCES

- [1] I. Repins, M. Contreras, B. Egaas, C. DeHart, J. Scharf, C. Perkins, B. To and R. Noufi, “19.9 % - efficient ZnO/CdS/CuInGaSe₂ solar cell with 81.2 % fill factor,” *Progress in Photovoltaics*, **16-3**, 235–239, 2008.
- [2] J. Palm, V. Probst, W. Stetter, R. Toelle, S. Visbeck, H. Calwer, T. Niesen, H. Vogt, O. Hernández, M. Wenl, F.H. Karg, “CIGS thin film PV modules: from fundamental investigations to advanced performance and stability”, *Thin Solid Films*, **451-452**, 544–551, 2004.
- [3] M. Powalla and B. Dimmler, “Process development of high performance CIGS modules for mass production”, *Thin Solid Films*, **387**, 251–256, 2001.
- [4] J. Song, S.S. Li, C.H. Huang, O.D. Crisalle and T.J. Anderson, “Device modelling and simulation of the performance of Cu(In_{1-x}Ga_x)Se₂ solar cells”, *Solid State Electronics*, **48**, 73–79, 2004.
- [5] M. Topič, F. Smole and J. Furlan, “Band-gap engineering in CdS/Cu(In,Ga)Se₂ solar cells”, *J. Appl. Phys.*, **79(11)**, 8537–8540, 1996.
- [6] M. Burgelman, P. Nollet and S. Degraeve, “Modelling polycrystalline semiconductor solar cells”, *Thin Solid Films*, **361-362**, 527–532, 2000.
- [7] S. Fonash, *Solar cell device physics*, Academic Press, 1981.
- [8] C. Snowden, *Introduction to semiconductor modelling*, World Scientific, 1986.
- [9] S. Selberherr, *Analysis and Simulation of Semiconductor Devices*, Springer Verlag, 1984.
- [10] M. Wolfe, N. Holonyak and G. Stillman, *Physical properties of semiconductors*, Prentice Hall, New-Jersey, 1989.
- [11] F. Dejene and V. Alberts, “Structural and optical properties of homogeneous Cu(In,Ga)Se₂ thin films prepared by thermal reaction of InSe/Cu/GaSe alloys with elemental Se vapour”, *J. Phys. D: Appl. Phys.*, **38**, 22–25, 2005.
- [12] W. Press, S. Teukolsky, W. Vetterling and B. Flannery, *Numerical recipes in C*, Cambridge University Press, 1995 (p. 226).
- [13] S. Adachi, *Optical properties of crystalline and amorphous semiconductors – Materials and fundamental principles*, Kluwer Academic Publishers, Boston, 1999 (p. 121).
- [14] M. Alonso, K. Wakita, J. Pascual, M. Garriga and N. Yamamoto, “Optical functions and electronic structure of CuInSe₂, CuGaSe₂, CuInS₂ and CuGaS₂”, *Phys. Rev. B*, **63**, 075203, 2001.
- [15] Jonas Malmström, *On generation and recombination in Cu(In,Ga)Se₂ thin-film solar cells*, Ph. D. thesis, University of Uppsala, 2005.
- [16] J. Krč, G. Černivec, A. Čampa, J. Malmström, M. Edoff, F. Smole and M. Topič, “Optical and